MICROPOLAR FORMULATION FOR REGULARIZATION OF MATERIAL INSTABILITIES IN SCALAR DAMAGE MODELS

Lapo Gori

Samuel Silva Penna

Roque Luiz da Silva Pitangueira

lapo@dees.ufmg.br

spenna@dees.ufmg.br

roque@dees.ufmg.br

Department of Structural Engineering, Federal University of Minas Gerais (UFMG)

Avenida Antônio Carlos, 6627, Pampulha, 31270-901, Belo Horizonte, MG, Brasil

Abstract. *Strain localization is an important issue in the numerical modelling of the physically non-linear behaviour of quasi-brittle materials. Scalar damage models, and the wider class of elastic-degrading models, commonly used for the representation of quasi-brittle media, may suffer for material instabilities due to their strain-softening behaviour. When analyzed numerically with the finite element method, a set of pathological phenomena may appear, hence affecting the quality of the simulations. The micropolar continuum formulation has been showed, in the past, to be a valid alternative for the mitigation of localization issues in elasto-plastic models and, recently, also in the case of scalar damage models. This papers aims to investigate the regularization properties of the micropolar theory when applied to a scalar damage model, and to evaluate the effects of the micropolar material parameters (the Cosserat's shear modulus and the internal bending length) on the onset of material instabilities. Analytical investigations are performed, in order to evaluate the onset of material instabilities with a proper localization indicator. Numerical simulations with the finite element method are also provided, in order to show the regularization properties of the adopted formulation.*

Keywords: *Micropolar continuum theory, Strain localization, Continuum damage mechanics*

1 INTRODUCTION

The simulation of the behaviour of *quasi-brittle* media, characterized by *strain-softening* constitutive models, is still a challenge for the different numerical methods, due to the phenomenon of strain localization. It is well known that numerical analyses of models where localization occours are characterized by a number of pathological behaviours, such as *strong mesh dependency*, *premature fracture initiation*, and *instantaneous perfectly-brittle fracture* (de Borst et al., 1993; Peerlings et al., 2002). When strain-softening materials models are adopted, at a certain load level the boundary value problem may become *ill-posed*, i.e., the equilibrium equations of the problem may loss their elliptic character. The ill-posedness of the problem corresponds to an infinite set of solutions, from which the numerical method selects the one corresponding to the smallest energy dissipation, resulting in mesh dependency problems.

The aforementioned pathological behaviours are due to a lack of the *local* description offered by the classic continuum theory in the representation of phenomena like damage and plasticity that are of *non-local* nature (Bazant, 1991). Common procedures consist in the use of *regularization methods* aiming to recover the non-local character of the phenomenon. An interesting overview on the different regularization methods con be found in de Borst et al. (1993) and Bažant and Jirásek (2002). Among the different alternatives there are: *non-local* and *gradient-enhanced* models (Bažant and Lin, 1988; Pijaudier-Cabot and Bažant, 1987; de Borst and Mühlhaus, 1992; Peerlings et al., 1996; Peerlings, 1999; Peerlings et al., 2001, 2002; Badnava et al., 2016), *viscous* models (Needleman, 1988), *cohesive zone* models (Dugdale, 1960; Barenblatt, 1962), and methods based on the *fracture energy approach* (Bažant and Oh, 1983). Important results have been obtained also with the *micropolar* continuum theory (Cosserat and Cosserat, 1909), which regularization properties have been investigated in a number of works, especially for the case of elasto-plastic media (de Borst and Sluys, 1991; de Borst, 1991; Sluys, 1992; Dietsche et al., 1993; Iordache and Willam, 1998; Xotta et al., 2016).

There are different approaches to the study of localization. Important informations on the phenomenon can be drawn from the theory of acceleration waves propagation (Hadamard, 1903; Hill, 1962), as well as from the quasi-static analysis of jump conditions in the strain rate at certain discontinuity surfaces of a body (Thomas, 1961; Rudnicki and Rice, 1975). Both the approaches lead to localization conditions that rely on the spectral properties of the *acoustic* (or localization) tensor, represented by the projection of the tangent constitutive operator along a certain direction (the local normal to the discontinuity surface). One is the weak localization condition, corresponding to the *loss of ellipticity* of the equilibrium equations, that depends directly on the acoustic tensor, while the other is the strong localization condition, also known as *loss of strong ellipticity*, which depends instead on the symmetric part of the acoustic tensor. Investigations in the field of elasto-plasticity have been performed by a number of authors, with works devoted to the analysis of the spectral properties of the acoustic tensor for the loss of ellipticity (Rice, 1976; Rice and Rudnicki, 1980; Ortiz, 1987; Borré and Maier, 1989; Bigoni and Hueckel, 1991a; Ottosen and Runesson, 1991b,a; Bigoni and Zaccaria, 1994), and of its symmetric part for the loss of strong ellipticity (Ottosen and Runesson, 1991b; Bigoni and Hueckel, 1991a; Bigoni and Zaccaria, 1992; Neilsen and Schreyer, 1993; Szabó, 2000). Regarding the field of elastic-degradation and damage models, only a few analytical investigations on localization phenomena have been performed (Desoyer and Cormery, 1994; Rizzi et al., 1995; Jirásek, 2007), mainly focused on *scalar-isotropic* damage models, with some works devoted to elastic degradation coupled with plasticity (Maier and Hueckel, 1979; Bigoni and Hueckel, 1991b).

However, taking advantage of a unified formulation (Carol et al., 1994; Rizzi et al., 1996; Rizzi and Carol, 2001), the theoretical and numerical resources developed for elasto-plasticity can be easily extended to damage models. An extensive treatise on the topic can be found in Rizzi (1995), where the different localization conditions, as well as the further failure indicators, are investigated for elastic-degrading models based on the classic continuum theory, with peculiar attention on scalar damage models.

Applications of the micropolar theory to damage models are rare in the literature, and are usually limited to scalar-isotropic damage models (Steinmann, 1995; Rahaman et al., 2015). A more comprehensive approach can be found in Gori et al. (2017b), where the authors proposed a general unified formulation for elastic degradation in micropolar media, able to represent also scalar-isotropic micropolar damage models. Also investigations of its regularization properties on damage models are a few: the work by Xotta et al. (2016) extended the procedures found in Iordache and Willam (1998) to the case of micropolar models with elasto-plastic behaviour coupled with scalar damage, while in Gori et al. (2017a) the authors extended the concepts of micropolar acceleration waves (Grioli, 1980; Eremeyev, 2005) to the case of micropolar elastic-degrading models (Gori et al., 2017b), in order to deriver proper localization measures for such models.

The present paper aims to enrich the results originally found in Gori et al. (2017b), adding to the analytical investigations performed in the mentioned paper also numerical analysis on the localization measures, and the effects on them of the Cosserat's material parameters. In the first part of the paper, the basic expressions of the micropolar theory are quickly recalled, together with the main expressions of a micropolar scalar damage model. Then, the formulation for localization analysis described in Gori et al. (2017a) is recasted for the specific case of an associated scalar damage model in a plane stress state (an extention to the micropolar theory of the model based on the strain energy proposed by Marigo (1985)). In the final part of the paper the results of the analysis are illustrated. First, an analytical investigation is performed for an uniaxial stress state. Then, the results of FEM simulations are used to perform the same localization analysis, based now on discrete results. The two investigations are compared, and the effects of the Cosserat's material parameters on the onset of localization are clearly showed.

1.1 Notations

Some standard notations used in the body of the paper are summarized here. The symbol $\mathbf{D} \subseteq \mathbf{E}$ indicates the domain of the body, i.e., a subset of the three-dimensional Euclidean space $\mathbf{E}$, in which the orthonormal basis $(\bar{e}_i)$ is defined. *Vectors* are indicated as $\bar{x} = x_i\ \bar{e}_i$, while *second-order* and *fourth-order* tensors respectively as $\underline{x} = x_{ij}\ \bar{e}_i \otimes \bar{e}_j$, and $\hat{\mathbf{x}} = x_{ijk\ell}\ \bar{e}_i \otimes \bar{e}_j \otimes \bar{e}_k \otimes \bar{e}_\ell$. The symbol $\cdot$ denotes both the standard dot product between vectors and the total contraction between tensors like, for example, $\bar{x}\cdot\bar{y} = x_i\, y_i$, $\underline{x}\cdot\bar{y} = x_{ij}\, y_j\, \bar{e}_i$, $\hat{\mathbf{x}}\cdot\underline{y} = x_{ijkl}\, y_{kl}\, \bar{e}_i\otimes\bar{e}_j$ and the other possible combinations. With the symbol $\otimes$, the standard tensorial product, as $\bar{x} \otimes \bar{y} = x_i\, y_j\, \bar{e}_i \otimes \bar{e}_j$ or $\underline{x} \otimes \underline{y} = x_{ij}\, y_{k\ell}\, \bar{e}_i \otimes \bar{e}_j \otimes \bar{e}_k \otimes \bar{e}_\ell$, is indicated. In the following of the paper, if not differently specified, spaces will be assumed to be three-dimensional and the latin indexes will run from 1 to 3; an exception is represented by the *generalized* quantities defined in six-dimensional spaces, for which the indices will run from 1 to 6.

2 MICROPOLAR MEDIA

In a geometrically-linear context, the configuration of a micropolar continuum is characterized, at each point of the domain **D**, by a *displacement field* $\bar{u}$ and a *micro-rotation field* $\bar{\varphi}$, leading to the strain measures

$$\underline{\gamma} = \mathrm{grad}^{\mathrm{T}}(\bar{u}) - \mathsf{e} \cdot \bar{\varphi} = (u_{j,i} - \mathsf{e}_{ijk}\, \varphi_k)\ \bar{e}_i \otimes \bar{e}_j \tag{1}$$

$$\underline{\kappa} = \mathrm{grad}^{\mathrm{T}}(\bar{\varphi}) = \varphi_{j,i}\, \bar{e}_i \otimes \bar{e}_j \tag{2}$$

which are referred to as *strain tensor* and *micro-curvature tensor*, respectively, and where the symbol e indicates the standard *Levi-Civita* operator with three indexes. To these strain measures correspond, respectively, the stress tensor $\underline{\sigma}$ and the couple-stress tensor $\underline{\mu}$ which must satisfy the local equilibrium equations for forces and moments in the domain **D**

$$\mathrm{div}^{\mathrm{T}}\,(\underline{\sigma}) + \bar{b} = \rho\ddot{\bar{u}} \longrightarrow \sigma_{ij,i} + b_j = \rho\ddot{u}_j \tag{3}$$

$$\mathrm{div}^{\mathrm{T}}\,\big(\underline{\mu}\big) + \mathsf{e} \cdot \underline{\sigma} + \bar{l} = \rho\theta\ddot{\bar{\varphi}} \longrightarrow \mu_{ij,i} + \mathsf{e}_{jkl}\,\sigma_{kl} + l_j = \rho\theta\ddot{\varphi}_j \tag{4}$$

where $\bar{b}$ and $\bar{l}$ represent volume forces and volume couples acting in the body domain, respectively, ρ is the density of the medium and $\rho\theta$ is the scalar measure of the rotation inertia of continuum particles (see, e.g., Eremeyev (2005)). To the previous equations, the following *natural* and *essential* boundary conditions are associated

$$\bar{\eta} \cdot \underline{\sigma} = \bar{t}_A \text{ at } \partial\mathbf{D}^u_n, \quad \bar{\eta} \cdot \underline{\mu} = \bar{t}_C \text{ at } \partial\mathbf{D}^\varphi_n \tag{5}$$

$$\bar{u} = \bar{u}^* \text{ at } \partial\mathbf{D}^u_e, \quad \bar{\varphi} = \bar{\varphi}^* \text{ at } \partial\mathbf{D}^\varphi_e \tag{6}$$

where $\bar{\eta}$ is the *unit normal vector field* defined at the boundary $\partial\mathbf{D}$ of the body, which parts are such that

$$\partial\mathbf{D}^u_n \cap \partial\mathbf{D}^u_e = \emptyset, \quad \partial\mathbf{D}^u_n \cup \partial\mathbf{D}^u_e = \partial\mathbf{D}, \quad \partial\mathbf{D}^\varphi_n \cap \partial\mathbf{D}^\varphi_e = \emptyset, \quad \partial\mathbf{D}^\varphi_n \cup \partial\mathbf{D}^\varphi_e = \partial\mathbf{D} \tag{7}$$

In the case of linear elasticity and disregarding the *membrane-bending coupling*, stress and deformation measures are linked by the following constitutive equations

$$\underline{\sigma} = \hat{\mathbf{A}}^0 \cdot \underline{\gamma}, \qquad \underline{\mu} = \hat{\mathbf{C}}^0 \cdot \underline{\kappa} \tag{8}$$

where $\hat{\mathbf{A}}^0$ and $\hat{\mathbf{C}}^0$ are the initial constitutive operators for the micropolar theory that, assuming an initially isotropic material, are expressed in terms of six material parameters as

$$\hat{\mathbf{A}}^0 = A^0_1\, \underline{id} \otimes \underline{id} + (A^0_2 + A^0_3)\, \hat{\mathbf{ID}}^{sym} + (A^0_2 - A^0_3)\, \hat{\mathbf{ID}}^{skw} \tag{9}$$

$$\hat{\mathbf{C}}^0 = C^0_1\, \underline{id} \otimes \underline{id} + (C^0_2 + C^0_3)\, \hat{\mathbf{ID}}^{sym} + (C^0_2 - C^0_3)\, \hat{\mathbf{ID}}^{skw} \tag{10}$$

where $\underline{id} = \delta_{ij}\ \bar{e}_i \otimes \bar{e}_j$ is the *identity tensor* in the space of second-order tensors, while $\hat{\mathbf{ID}}^{sym}$ and $\hat{\mathbf{ID}}^{skw}$ are, respectively, the *symmetric* and *skew-symmetric* identity tensors in the space of fourth-order tensors, such that $\hat{\mathbf{ID}}^{sym} \cdot \underline{x} = \underline{x}^{sym}$ and $\hat{\mathbf{ID}}^{skw} \cdot \underline{x} = \underline{x}^{skw}$, defined as

$$\hat{\mathbf{ID}}^{sym} := \frac{1}{2}\left(\delta_{ik}\delta_{j\ell} + \delta_{i\ell}\delta_{jk}\right)\ \bar{e}_i \otimes \bar{e}_j \otimes \bar{e}_k \otimes \bar{e}_\ell \tag{11}$$

$$\hat{\mathbf{ID}}^{skw} := \frac{1}{2}\left(\delta_{ik}\delta_{j\ell} - \delta_{i\ell}\delta_{jk}\right)\ \bar{e}_i \otimes \bar{e}_j \otimes \bar{e}_k \otimes \bar{e}_\ell \tag{12}$$

2.1 Associated scalar-isotropic damage

Following Gori et al. (2015, 2017b,a), a scalar-isotropic micropolar damage model is expressed by the following stress and couple-stress rates

$$\underline{\dot{\sigma}} = \left((1-D)\, \hat{\mathbf{A}}^0 - \frac{\partial D(\Gamma_{eq})}{\partial \Gamma_{eq}} \left(\underline{\sigma}^0 \otimes \frac{\partial \Gamma_{eq}}{\partial \underline{\gamma}} \right) \right) \cdot \underline{\dot{\gamma}} - \frac{\partial D(\Gamma_{eq})}{\partial \Gamma_{eq}} \left(\underline{\sigma}^0 \otimes \frac{\partial \Gamma_{eq}}{\partial \underline{\kappa}} \right) \cdot \underline{\dot{\kappa}} \quad (13)$$

$$\underline{\dot{\mu}} = \left((1-D)\, \hat{\mathbf{C}}^0 - \frac{\partial D(\Gamma_{eq})}{\partial \Gamma_{eq}} \left(\underline{\mu}^0 \otimes \frac{\partial \Gamma_{eq}}{\partial \underline{\kappa}} \right) \right) \cdot \underline{\dot{\kappa}} - \frac{\partial D(\Gamma_{eq})}{\partial \Gamma_{eq}} \left(\underline{\mu}^0 \otimes \frac{\partial \Gamma_{eq}}{\partial \underline{\gamma}} \right) \cdot \underline{\dot{\gamma}} \quad (14)$$

where $\Gamma_{eq} = \Gamma_{eq}(\underline{\gamma}, \underline{\kappa})$ is the so-called *equivalent deformation*, a functions depending on both the strain and curvature tensors representing the current loading condition of a model, D is a *scalar damage variable* (assumed to vary from 0, undamaged material, to 1, completely damaged material) whose evolution is described by the function $D(\Gamma_{eq})$, and $\underline{\sigma}^0$ and $\underline{\mu}^0$ are defined as $\underline{\sigma}^0 := \hat{\mathbf{A}}^0 \cdot \underline{\gamma}$ and $\underline{\mu}^0 := \hat{\mathbf{C}}^0 \cdot \underline{\kappa}$. The previous equation can be represented in a compact form (Gori et al., 2017b) using the *generalized tangent operator* $\hat{\mathcal{E}}^t$ as

$$\underline{\dot{\Sigma}} = \hat{\mathcal{E}}^t \cdot \underline{\dot{\Gamma}}, \qquad \hat{\mathcal{E}}^t = (1-D)\, \hat{\mathcal{E}}^0 - \frac{\partial D(\Gamma_{eq})}{\partial \Gamma_{eq}}\, \underline{\Sigma}^0 \otimes \frac{\partial \Gamma_{eq}}{\partial \underline{\Gamma}} \quad (15)$$

with

$$\underline{\Sigma}^0 = \begin{pmatrix} \underline{\sigma}^0 & \underline{0} \\ \underline{0} & \underline{\mu}^0 \end{pmatrix}, \qquad \frac{\partial \Gamma_{eq}}{\partial \underline{\Gamma}} = \begin{pmatrix} \frac{\partial \Gamma_{eq}}{\partial \underline{\gamma}} & \underline{0} \\ \underline{0} & \frac{\partial \Gamma_{eq}}{\partial \underline{\kappa}} \end{pmatrix} \quad (16)$$

A peculiar class of scalar-isotropic damage models is represented by the ones *associated in the strain-space*, characterized by $\partial \Gamma_{eq} / \partial \underline{\Gamma} = \beta\, \underline{\Sigma}^0$, where the parameter β depends on the peculiar damage model. In this case, the generalized tangent operator assumes the expression

$$\hat{\mathcal{E}}^t = (1-D)\, \hat{\mathcal{E}}^0 - \beta \frac{\partial D(\Gamma_{eq})}{\partial \Gamma_{eq}}\, \underline{\Sigma}^0 \otimes \underline{\Sigma}^0 \quad (17)$$

In this paper, an extention to the micropolar theory of the damage model based on the strain energy proposed by Marigo (1985) is considered, characterized by

$$\Gamma_{eq} = \sqrt{\frac{2\psi^0}{E^0}}, \quad \psi_0 = \frac{1}{2}\, \underline{\gamma} \cdot \left(\hat{\mathbf{A}}^0 \cdot \underline{\gamma} \right) + \frac{1}{2}\, \underline{\kappa} \cdot \left(\hat{\mathbf{C}}^0 \cdot \underline{\kappa} \right), \quad \beta = \frac{1}{E^0\, \Gamma_{eq}} \quad (18)$$

together with the exponential damage law

$$D(\Gamma_{eq}) = 1 - \frac{K_0}{\Gamma_{eq}} \left(1 - \tau + \tau e^{-\xi(\Gamma_{eq} - K_0)} \right) \quad (19)$$

where K_0 is a threshold value for the equivalent deformation, representing the onset of damage, and where τ and ξ are parameters that allow to control, respectively, the maximum value of the scalar damage variable and the damage evolution intensity.

3 LOCALIZATION ANALYSIS

Localization in micropolar scalar damage models has been investigated by Gori et al. (2017a) in terms of acceleration waves propagation. An acceleration wave in a micropolar medium is represented by a wave trasporting a second-order discontinuity in the displacement field $\bar{u}$ and in the micro-rotation field $\bar{\varphi}$ (Eremeyev, 2005), which moves relatively to the material with a velocity c in its normal direction $\bar{n}$. According to the authors, localization verifies when the wavefront became *stationary* for a certain direction $\bar{n}$. In that case, across the wavefront the strain and micro-curvature rates present a discontinuity expressed by the *Maxwell compatibility conditions* as (the symbol $[\![a]\!] := a^+ - a^-$ indicates the jump of a field variable a across the wavefront, and the symbols a^+ and a^- indicate the values of the same field variable at the opposite sides of the discontinuity surface)

$$[\![\dot{\underline{\gamma}}]\!] = \bar{n} \otimes \bar{g}_A, \qquad [\![\dot{\underline{\kappa}}]\!] = \bar{n} \otimes \bar{g}_C \tag{20}$$

There, the vectors $\bar{g}_A$ and $\bar{g}_C$ are expressed by $\bar{g}_A = \dot{\gamma}_A \bar{p}_A$ and $\bar{g}_C = \dot{\gamma}_C \bar{p}_C$, where $\dot{\gamma}_A := \|\bar{g}_A\|$ and $\dot{\gamma}_C := \|\bar{g}_C\|$ represent the magnitude of the jumps, while the unitary vectors $\bar{p}_A := \bar{g}_A/\|\bar{g}_A\|$ and $\bar{p}_C := \bar{g}_C/\|\bar{g}_C\|$ are the polarization vectors, i.e., the vectors defining the motion of the material points on the discontinuity surface in terms of displacement and micro-rotation, respectively. Furthermore, the jumps in the stress and couple-stress rates must satisfy the *traction rate continuity conditions*, expressed by

$$\bar{n} \cdot [\![\dot{\underline{\sigma}}]\!] = \bar{0}, \qquad \bar{n} \cdot [\![\dot{\underline{\mu}}]\!] = \bar{0} \tag{21}$$

Making use of both the Maxwell compatibility conditions and the traction rate continuity conditions, the rate equilibrium equations Eqs. (13) and (14) at the discontinuity surface (i.e., written in terms of $[\![\dot{\underline{\sigma}}]\!]$, $[\![\dot{\underline{\mu}}]\!]$, $[\![\dot{\underline{\gamma}}]\!]$ and $[\![\dot{\underline{\kappa}}]\!]$) can be expressed as

$$\underline{Q}^t_{AA} \cdot \bar{g}_A + \underline{Q}^t_{AC} \cdot \bar{g}_C = \bar{0} \tag{22}$$
$$\underline{Q}^t_{CA} \cdot \bar{g}_A + \underline{Q}^t_{CC} \cdot \bar{g}_C = \bar{0} \tag{23}$$

where the following *tangent acoustic tensors* have been introduced

$$\underline{Q}^t_{AA} := (1-D)\,\underline{Q}^0_{AA} - \frac{\beta}{H}\,\bar{b}_A \otimes \bar{b}_A, \qquad \underline{Q}^t_{AC} := -\frac{\beta}{H}\,\bar{b}_A \otimes \bar{b}_C \tag{24}$$
$$\underline{Q}^t_{CC} := (1-D)\,\underline{Q}^0_{CC} - \frac{\beta}{H}\,\bar{b}_C \otimes \bar{b}_C, \qquad \underline{Q}^t_{CA} := -\frac{\beta}{H}\,\bar{b}_C \otimes \bar{b}_A \tag{25}$$

with the *elastic acoustic tensors* and the *traction vectors* defined as (Hill, 1962)

$$\underline{Q}^0_{AA} := \left(n_k A^0_{ki\ell j} n_\ell\right)\,\bar{e}_i \otimes \bar{e}_j, \quad \underline{Q}^0_{CC} := \left(n_k C^0_{ki\ell j} n_\ell\right)\,\bar{e}_i \otimes \bar{e}_j \tag{26}$$
$$\bar{b}_A := \bar{n} \cdot \underline{\sigma}^0, \quad \bar{b}_C := \bar{n} \cdot \underline{\mu}^0 \tag{27}$$

Eqs. (22) and (22) can be recasted in a compact form as

$$\underline{Q}^t \cdot \bar{g} = \bar{0}, \qquad \underline{Q}^t = (1-D)\,\underline{Q}^0 - \frac{\beta}{H}\left(\bar{b} \otimes \bar{b}\right) \tag{28}$$

where

$$\underline{Q}^t := \begin{pmatrix} \underline{Q}^t_{AA} & \underline{Q}^t_{AC} \\ \underline{Q}^t_{CA} & \underline{Q}^t_{CC} \end{pmatrix}, \quad \underline{Q}^0 := \begin{pmatrix} \underline{Q}^0_{AA} & \underline{0} \\ \underline{0} & \underline{Q}^0_{CC} \end{pmatrix}, \quad \bar{b} := \begin{pmatrix} \bar{b}_A \\ \bar{b}_C \end{pmatrix}, \quad \bar{g} := \begin{pmatrix} \bar{g}_A \\ \bar{g}_C \end{pmatrix} \tag{29}$$

Localization is possible when Eq. (28) is satisfied for a certain normal direction $\bar{n}$ and polarization direction $\bar{g}$, i.e., when $\det\left(\underline{\mathrm{Q}}^{\mathrm{t}}\right) = 0$. Instead of calculating directly the determinant of the acoustic tensor, the onset of localization is usually evaluated with an alternative condition (see, e.g., Rizzi et al. (1996)). Introducing the tensor $\underline{D}$ such that $\underline{D} := (\underline{Q}^0)^{-1}\underline{Q}^t/(1-D)$, it follows that the condition $\det\left(\underline{\mathrm{Q}}^{\mathrm{t}}\right) = 0$ is equivalent to $\det\left(\underline{\mathrm{D}}\right) = \det\left(\underline{\mathrm{Q}}^{\mathrm{t}}\right)/((1-D)\det\left(\underline{\mathrm{Q}}^{0}\right)) = 0$. Introducing the *localization indicator* $q := \det\left(\underline{\mathrm{D}}\right)$ that, according to the matrix determinant lemma (see, e.g., Ding and Zhou (2007)), is expressed by

$$q = 1 - \frac{\beta}{(1-D)\,H}\left[\bar{b}_A \cdot \left((\underline{Q}^0_{AA})^{-1} \cdot \bar{b}_A\right) + \bar{b}_C \cdot \left((\underline{Q}^0_{CC})^{-1} \cdot \bar{b}_C\right)\right] \tag{30}$$

the onset of localization is now attained when $q = 0$.

Assuming a plane-stress state in the plane (x,y), the displacement and micro-rotation vectors, the polarization vectors, and the direction of propagation reduce to

$$\bar{u} = \begin{pmatrix} u_x \\ u_y \end{pmatrix}, \quad \bar{\varphi} = \begin{pmatrix} \varphi_z \end{pmatrix}, \quad \bar{p}_A = \begin{pmatrix} p_{Ax} \\ p_{Ay} \end{pmatrix}, \quad \bar{p}_C = \begin{pmatrix} 1 \end{pmatrix}, \quad \bar{n} = \begin{pmatrix} n_x \\ n_y \end{pmatrix} \tag{31}$$

and the elastic isotropic constitutive relation can be recasted, in Voigt notation, as

$$\begin{pmatrix} \sigma_{xx} \\ \sigma_{xy} \\ \sigma_{yx} \\ \sigma_{yy} \\ \mu_{xz} \\ \mu_{yz} \end{pmatrix} = \begin{pmatrix} \frac{E^0}{1-\nu^2} & 0 & 0 & \frac{\nu E^0}{1-\nu^2} & 0 & 0 \\ 0 & G^0+\alpha^0 & G^0-\alpha^0 & 0 & 0 & 0 \\ 0 & G^0-\alpha^0 & G^0+\alpha^0 & 0 & 0 & 0 \\ \frac{\nu E^0}{1-\nu^2} & 0 & 0 & \frac{E^0}{1-\nu^2} & 0 & 0 \\ 0 & 0 & 0 & 0 & 2GL_b^2 & 0 \\ 0 & 0 & 0 & 0 & 0 & 2GL_b^2 \end{pmatrix} \begin{pmatrix} \gamma_{xx} \\ \gamma_{xy} \\ \gamma_{yx} \\ \gamma_{yy} \\ \kappa_{xz} \\ \kappa_{yz} \end{pmatrix} \tag{32}$$

where E^0 is the initial Young's modulus, G^0 the initial shear modulus, ν the Poisson's ratio (that, as for scalar isotropic damage in classic media, is not modified by the scalar damage variable), α^0 the initial Cosserat's shear modulus (as defined in the previous section), and L_b the internal bending length, that in a plane-stress state satisfies the equality $GL_b = C_2$. These equations lead to the following expressions for the initial acoustic tensors

$$\underline{Q}^0_{AA} = \begin{pmatrix} G^0+\alpha^0 & 0 \\ 0 & G^0+\alpha^0 \end{pmatrix} + \left(\frac{\nu E^0}{1-\nu^2} + G^0 - \alpha^0\right)\begin{pmatrix} n_x^2 & n_x n_y \\ n_x n_y & n_y^2 \end{pmatrix} \tag{33}$$

$$\underline{Q}^0_{CC} = 2G^0 L_b^2 \tag{34}$$

and for their inverse

$$\left(\underline{Q}^0_{AA}\right)^{-1} = \begin{pmatrix} \frac{1}{G^0+\alpha^0} & 0 \\ 0 & \frac{1}{G^0+\alpha^0} \end{pmatrix} - \frac{\chi}{G^0+\alpha^0} \begin{pmatrix} n_x^2 & n_x n_y \\ n_x n_y & n_y^2 \end{pmatrix} \tag{35}$$

$$\left(\underline{Q}^0_{CC}\right)^{-1} = \frac{1}{2G^0 L_b^2} \tag{36}$$

where the material parameter

$$\chi := \left(\frac{\nu E^0}{1-\nu^2} + G^0 - \alpha^0\right) \frac{1-\nu^2}{E^0} \tag{37}$$

has been introduced. Replacing these values into Eq. (30), the expression of the localization indicator became

$$q = 1 - \frac{\beta}{(1-D)\,H} \left[\frac{1}{G^0+\alpha^0}\left(\bar{b}_A \cdot \bar{b}_A - \chi(\bar{n}\cdot\bar{b}_A)^2\right) + \frac{1}{2G^0 L_b^2}\bar{b}_C \cdot \bar{b}_C\right] \tag{38}$$

4 RESULTS

The present section is devoted to the investigation of the effects of the Cosserat's material parameters on the onset of localization. The contents of the previous sections are used to obtain both analytical and numerical results regarding the localization effects; the latters have been obtained with FEM simulations. The FEM simulations presented in this paper have been performed with the open-source software *INSANE* (INteractive Structural ANalysis Environment, `http://www.insane.dees.ufmg.br`), which source code is freely available at the Git repository `https://git.insane.dees.ufmg.br/insane/insane.git`.

4.1 Uniaxial stress state: analytical considerations

An uniaxial stress state in absence of couple-stresses is considered (Gori et al., 2017a), with the only non-zero component of the stress tensor $\underline{\sigma}^0$ assumed to be σ^0_{yy}; this assumption results in $\Gamma_{eq} = \gamma_{yy} = \sigma^0_{yy}/E^0$ and $\beta = 1/\sigma^0_{yy}$. From Eq. (38), the localization indicator assumes the expression

$$q = 1 - \frac{\sigma^0_{yy}}{(1-D)(G^0+\alpha^0)\,H}\left(n_y^2 - \chi\, n_y^4\right) \tag{39}$$

where n_y is the projection of the direction of propagation onto the y axis. In order to perform the analysis, a specific material is considered, with Young's modulus E = 20000 N/mm^2, Poisson's ratio ν = 0.30 and shear modulus G = 7692.31 N/mm^2, with the following parameters for the exponential damage law, τ = 0.999, ξ = 500 and K$_0$ = 5×10^{-5}. The effect of the micropolar parameters is evaluated considering three different values for the Cosserat's shear modulus: α = 0 N/mm^2, in order to reproduce the limit case of a classic medium, α = 500 N/mm^2 and α = 2500 N/mm^2. Fig. 1 presents the results of the analysis in terms of the localization indicator for the different values of the Cosserat's shear modulus at the onset of damage (i.e., with $D \simeq 0$). There, the localization indicator is plotted against the angle θ_n between the propagation direction and the y axis ($n_y = \cos(\theta_n)$). As showed in the figure, the Cosserat's shear modulus

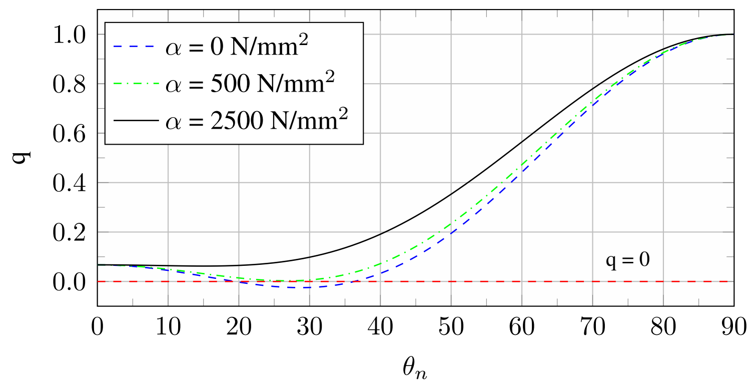

Figure 1: Localization indicator

influences the onset of localization; for both α = 0 N/mm^2 and α = 500 N/mm^2 the localization condition is attained as soon as damage initiates, for certain directions of propagation, while the case with α = 2500 N/mm^2 verifies the condition $q > 0$ for all the possible directions.

Despite the results of Fig. 1 may offer important informations on the possibility of formation of localized solutions, it should be noted that they are valid under the hypothesis of uniaxial stress state, which is lost once the damage initiates.

4.2 Symmetric plate

The analysis performed in the previous section allowed to show the role of the Cosserat's shear modulus on the onset of localization. Such analytical results can be also confirmed numerically, using a FEM simulation. The square panel of Fig. 2 is considered. The material parameters are the same as defined before, except for two symmetric weakened zones (the hatched areas in 2) presenting a reduction in the parameter K$_0$; the role of these imperfections is to trigger a bifurcated solution once the localization condition is met. Due to the boundary conditions of the plate, prior to damage initiation its stress state is uniaxial; hence a direct comparison with the previous analytical results can be made.

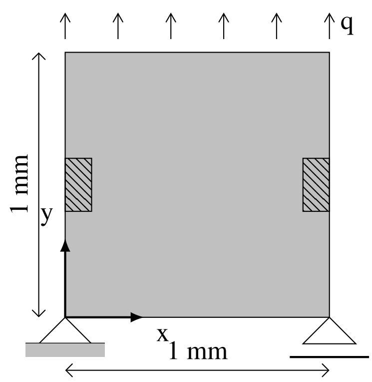

Figure 2: Square panel

The square panel is modelled with four-nodes elements in a plane-stress state, with a thickness of 1 mm. The loading process is driven by the *generalized displacement control method* (Yang and Shieh, 1990), assuming a reference load q = 1 N/mm, an initial loading factor increment of 0.005, and a tollerance for the convergence on the relative displacement of 1×10^{-4}.

Three different meshes are considered with 100, 400 and 1600 elements; the weakend zones have the same dimensions for the three meshes. For each mesh the analysis is repeated using the three different values of the Cosserat's shear modulus defined for the analytical considerations on the localization indicators. Regarding the internal bending length, a set of simulations has been performed considering a unitary value (L_b = 1.0 mm) in combination with the three values of the parameter α, while in another set of simulations its value has been reduced to L_b = 0.1 mm, in combination with α = 2500 N/mm^2. Despite the fact that the internal bending length doesn't have an active role on the analytical considerations (indeed it doesn't appear in Eq. (39)), it is remarked that, as stated before, once the damage initiates the solution is no more uniform and the uniaxial stress state is lost; hence, couple-stresses may appear, activating the internal bending length.

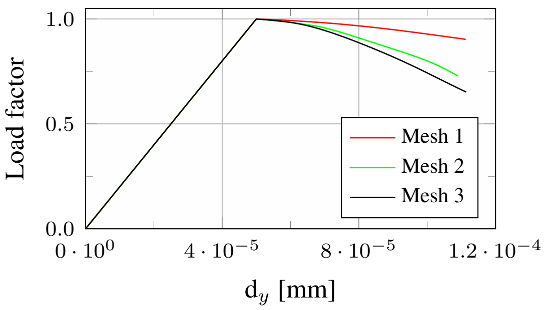

(a) α = 0 N/mm^2 - L_b = 1.0 mm

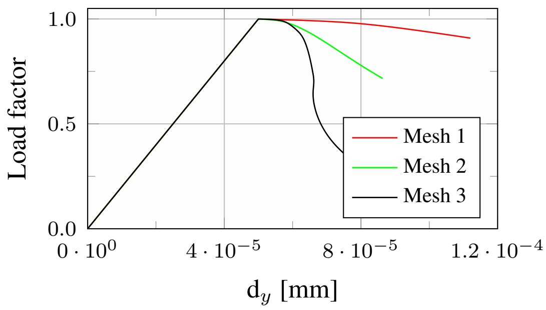

(b) α = 500 N/mm^2 - L_b = 1.0 mm

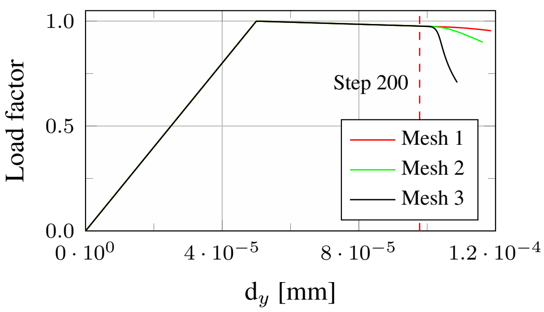

(c) α = 2500 N/mm^2 - L_b = 1.0 mm

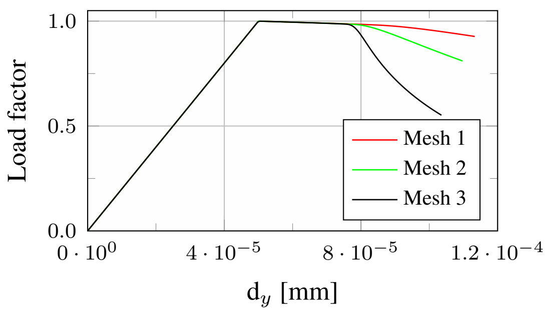

(d) α = 2500 N/mm^2 - L_b = 0.1 mm

Figure 3: Equilibrium paths

In Fig. 3 the results of the analyses are reported in terms of equilibrium paths, with the vertical displacement plotted against the load factor. The first two combinations of material parameters (Figs. 3(a) and 3(b)), the ones which fulfill the localization condition since damage initiation (Fig. 1), show solutions that don't converge under mesh refinement, and that, in general, may vary if a simulation is repeated. The third combination (Fig. 3(c)), for which the localization indicator is still positive at damage initiation, shows instead the same equilibrium path for the different meshes. The solution is the same up to a value of the vertical displacement of approximately 1.0×10^{-4} mm, after which the three paths diverge. The same behaviour is presented by the last combination, the one with the reduced value of the internal bending length; the only difference is represented by the presence of a divergence in the equilibrium path for a lower value of the vertical displacement.

These results match with the previous analytical considerations, showing the the localization indicator of Eq. (39) is indeed a valid warning for the presence of bifurcated solutions. The same indicator however, is not able to detect the divergence in the equilibrium paths showed in Figs. 3(c) and 3(d) after a certain value of the vertical displacement. As observed in Gori et al. (2017a), such divergence corresponds to a mode-I failure of the panel where the deformations concentrates in a single horizontal band of elements. For high values of the Cosserat's shear modulus this is the only possible failure; as showed in Fig. 1, as α grows the value of q at $\theta_n = 0$ tends to be the lower one, i.e., the most critical condition. Despite the localization condition is not met at damage initiation, during the loading process the stress state diverges from the uniaxial one and the values of the localization indicator may be locally lower than the expected ones. Here it is emphasized the role of the internal bending length that, as stated before, is activated once couple-stresses arise. As it can be observed in Fig. 3(c), the higher value of L_b allows to prevent the mode-I localized failure up to a value of the vertical displacement higher than the one that has been attained in Fig. 3(d).

Further informations on the localized failure that may interest the considered model can be draw performing the same localization analysis using the real stress state of the model rather than an ideal uniaxial one. At each integration point of the different FEM meshes, the localization analysis has been performed using the state variables calculated during the loading process. The localization indicator has been calculated using Eq. (38), by varying the direction $\bar{n}$ in order to find its minimum value at each point. The results of the discrete localization analysis are resumed in Figs. 4 to 6 for the finer mesh, where the contour plots have been obtained using the *Python* library *Matplotlib* (Hunter, 2007). Together with the localization indicator, also the distribution of the scalar damage variable in the plate is plotted.

In Fig. 4, the condition at the onset of damage is considered (step 11 of the analysis). As it can be observed, the first two combinations of material parameters are such that the localization indicator already presents negative values at the onset of damage, as predicted by the analytical study. Regarding the damage distribution, it can be observed that it tends to concentrate in the most internal band of elements and into four inclined branches. The other two combinations on the contrary, present a localization indicator that is positive on the whole domain, confirming the analytical prediction. As it can be observed, the different values of the internal bending length don't have a significant influence on both the damage and localization indicator distribution at this stage of the loading process.

Fig. 5 illustrates the situation of the plate just after the onset of damage (step 15). As showed in Figs. 3(a) and 3(b), at this stage the first two sets of material parameters present divergent equilibrium paths already. The localization indicator is still negative on large part of the domain, and the damage tends to concentrate in inclined bands. As observed in Gori et al. (2017a) such bands are not deterministic, in the sense that they may vary from a simulation to another, resulting also in asymmetric branches. Furthermore, it can be observed that, due to the concentration of the damage in finite bands, parts of the domain are subjected to an unloading process. The models with the higher value of the Cosserat's shear modulus, at this stage, still present convergent equilibrium paths (Figs. 3(c) and 3(d)). The localization indicator is still positive, with the lower values concentrated in the most damaged areas.

The last figure (Fig. 6) illustrates the state of the plate at the step 200 of the four simulations which, for the combination with α = 2500 N/mm^2 and L_b = 1.0 mm, corresponds to a vertical displacement of 9.78 $\times$ 10^{-5} mm (Fig. 3(c)). From Fig. 3(c) it can be seen that at this stage, this combination of material parameters is the only one that still presents convergent equilib-

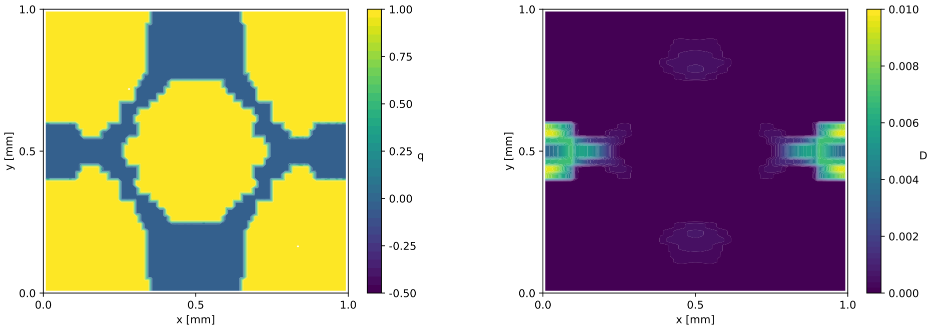

(a) α = 0 N/mm^2 - L$_b$ = 1.0 mm

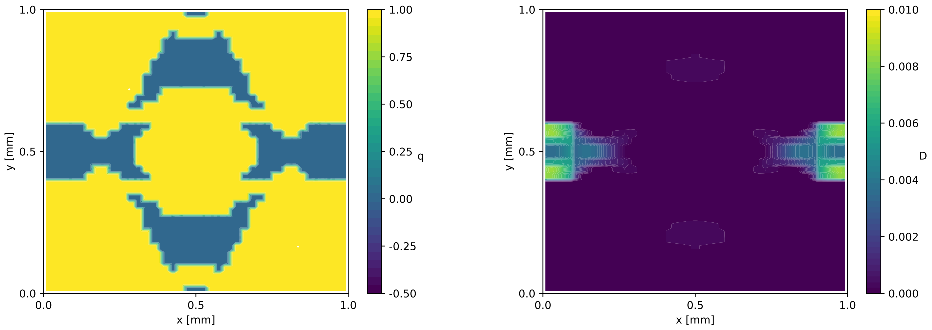

(b) α = 500 N/mm^2 - L$_b$ = 1.0 mm

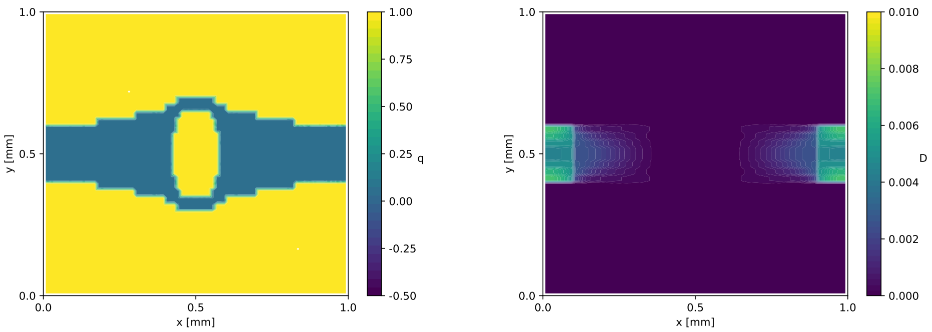

(c) α = 2500 N/mm^2 - L$_b$ = 1.0 mm

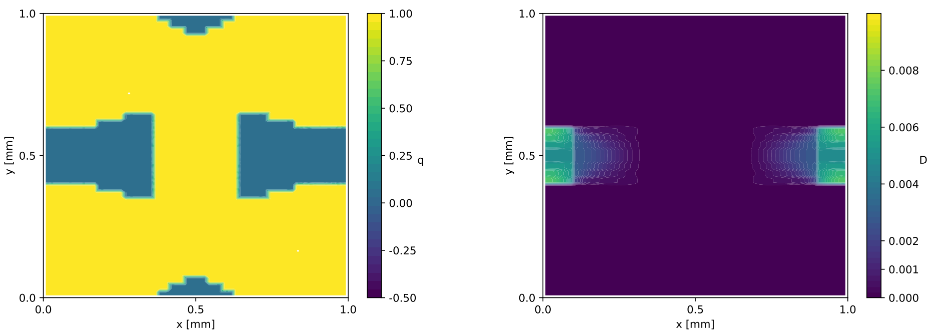

(d) α = 2500 N/mm^2 - L$_b$ = 0.1 mm

Figure 4: Localization indicator and damage variable - Mesh 3 - Step 11

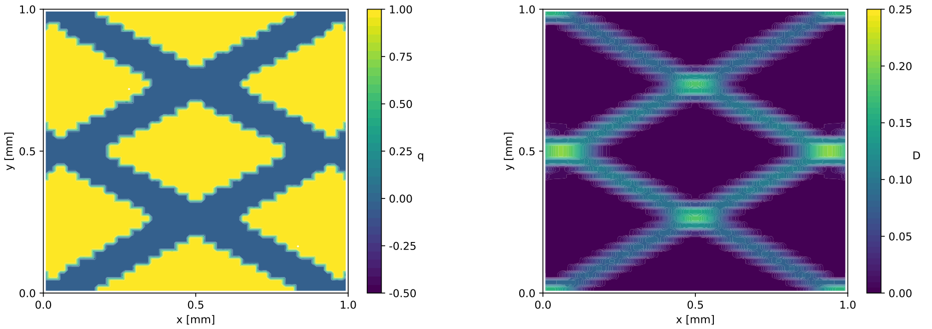

(a) α = 0 N/mm^2 - L$_b$ = 1.0 mm

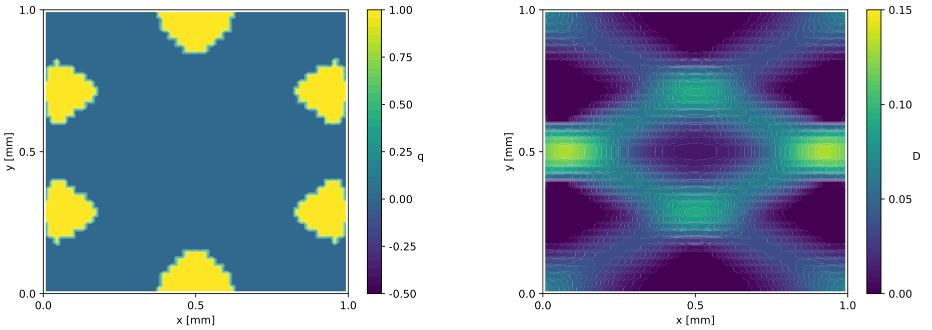

(b) α = 500 N/mm^2 - L$_b$ = 1.0 mm

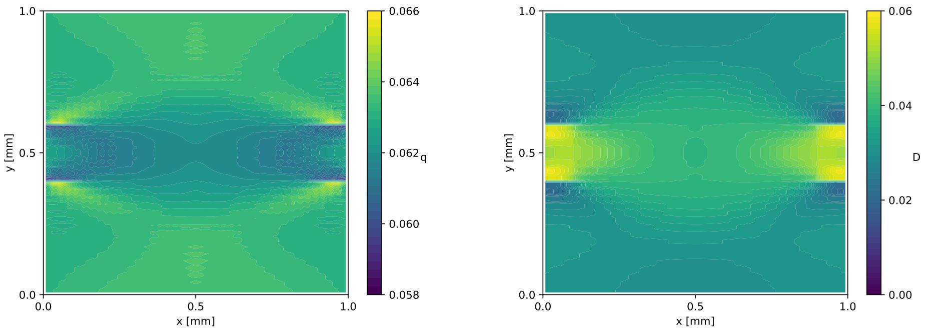

(c) α = 2500 N/mm^2 - L$_b$ = 1.0 mm

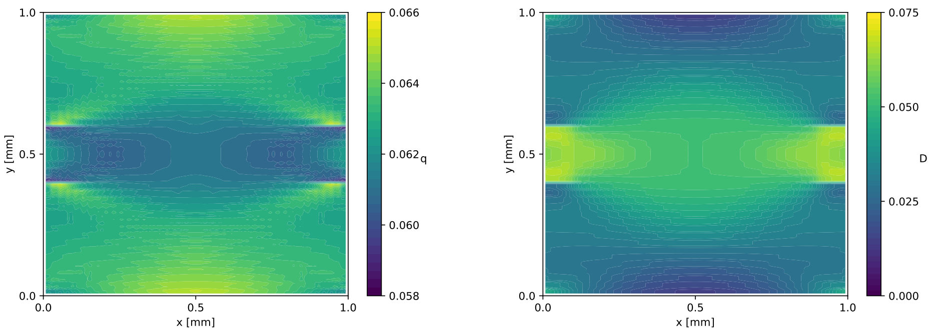

(d) α = 2500 N/mm^2 - L$_b$ = 0.1 mm

Figure 5: Localization indicator and damage variable - Mesh 3 - Step 15

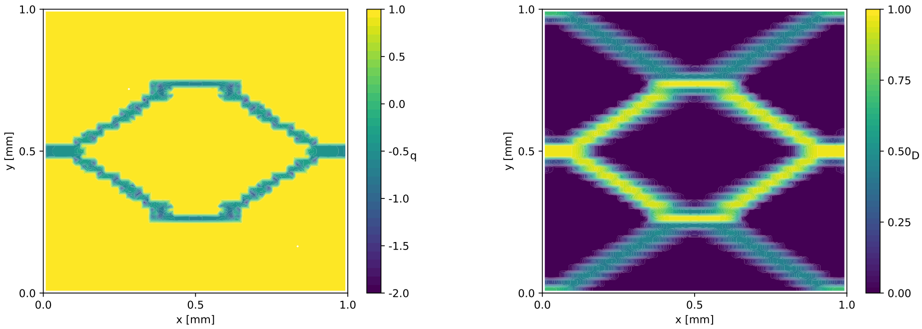

(a) $\alpha = 0$ N/mm^2 - L$_b$ = 1.0 mm

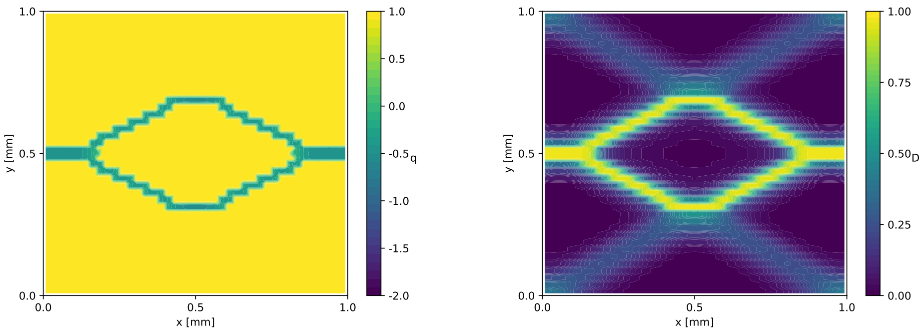

(b) $\alpha = 500$ N/mm^2 - L$_b$ = 1.0 mm

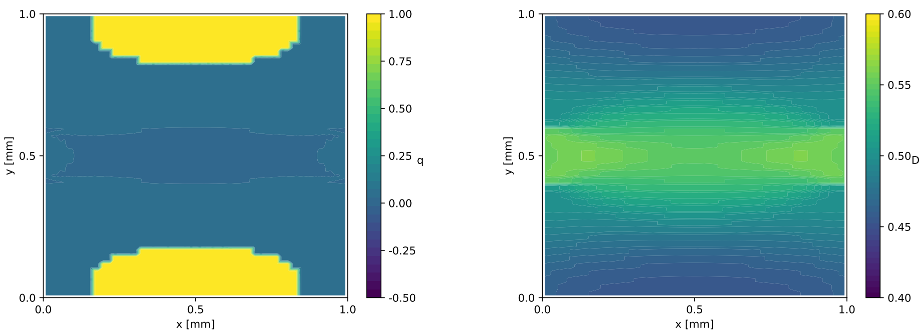

(c) $\alpha = 2500$ N/mm^2 - L$_b$ = 1.0 mm

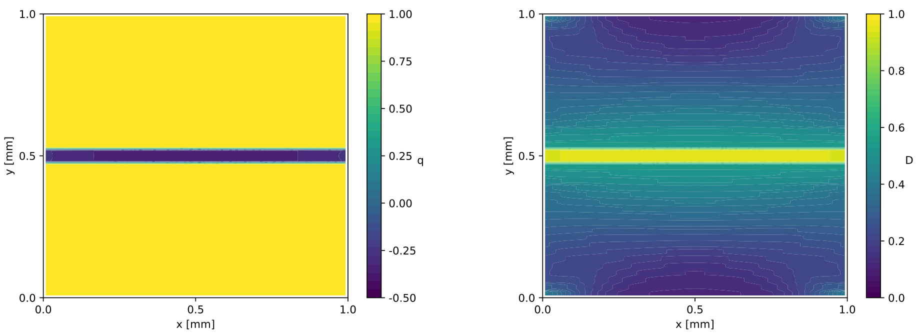

(d) $\alpha = 2500$ N/mm^2 - L$_b$ = 0.1 mm

Figure 6: Localization indicator and damage variable - Mesh 3 - Step 200

rium paths. However, it can be observe that the distribution of the localization indicator is quite different from the one of step 15, with negative values appearing in some parts of the domain. Since the localization condition is met, the subsequent steps of the analysis present divergent equilibrium paths (Fig. 3(c)), indicating the formation of a mode-I localized failure. The situation is analogous for the model with α = 2500 N/mm^2 and L_b = 0.1 mm. However, in this case the localization condition is met long before step 200 (Fig. 3(d)); at this stage, indeed, the model already presents the mode-I failure, with the damage trapped in the most internal band of elements (Fig. 6(d)). The other sets of materials parameters still present negatives values of the localization indicator, with damaged bands maintaining the same shape of the previous steps.

5 CONCLUSION

The regularization effects of the micropolar continuum theory have been investigated, considering a peculiar associated scalar damage model. The analytical results treated in a previous paper have been extended with a discrete localization analysis. The previous results have been confirmed by such analysis, that also helped to interpret some pathological behaviours of FEM simulations that the mere analytical investigation was not able to predict. The results illustrated in this paper allow to state that the micropolar formulation constitutes a valid alternative for the simulation of quasi-brittle materials represented in terms of damage models, as it has been shown to be in the past for elasto-plastic materials.

ACKNOWLEDGEMENTS

The first author (CNPq Scholarship - Brazil) and the other authors gratefully acknowledge the support of the brazilian research agencies FAPEMIG (in portuguese: *Fundação de Amparo à Pesquisa do Estado de Minas Gerais* - grant PMM-00669-15) and CNPq (in portuguese: *Conselho Nacional de Desenvolvimento Científico e Tecnológico* - grant 308785/2014-2).

REFERENCES

Badnava, H., Mashayekhi, M., & Kadkhodaei, M., 2016. An anisotropic gradient damage model based on microplane theory. *International Journal of Damage Mechanics*, vol. 25, n. 3, pp. 336–357.

Barenblatt, G. I., 1962. The mathematical theory of equilibrium cracks in brittle fracture. *Advances in Applied Mechanics*, vol. 7, pp. 55–129.

Bažant, P. Z. & Jirásek, M., 2002. Nonlocal integral formulations of plasticity and damage: survey of progress. *Journal of Engineering Mechanics*, vol. 128, n. 11, pp. 1119–1149.

Bažant, P. Z. & Lin, F. B., 1988. Non-local yield limit degradation. *International Journal for Numerical Methods in Engineering*, vol. 26, pp. 1805–1823.

Bažant, Z. P. & Oh, B. H., 1983. Crack band for fracture of concrete. *Materials and Structures*, vol. 16, n. 93, pp. 155–177.

Bazant, P. Z., 1991. Why continuum damage is nonlocal: micromechanics arguments. *Journal of Engineering Mechanics*, vol. 117, n. 5, pp. 1070–1087.

Bigoni, D. & Hueckel, T., 1991a. Uniqueness and localization - I Associative and non-associative elastoplasticity. *International Journal of Solids and Structures*, vol. 28, n. 2, pp. 197–213.

Bigoni, D. & Hueckel, T., 1991b. Uniqueness and localization - II Coupled elastoplasticity. *International Journal of Solids and Structures*, vol. 28, n. 2, pp. 215–224.

Bigoni, D. & Zaccaria, D., 1992. Loss of strong ellipticity in non-associative elastoplasticity. *Journal of the Mechanics and Physics of Solids*, vol. 40, n. 6, pp. 1313–1331.

Bigoni, D. & Zaccaria, D., 1994. On the eigenvalues of the acoustic tensor in elastoplasticity. *European Journal of Mechanics A/Solids*, vol. 13, n. 5, pp. 621–638.

Borré, G. & Maier, G., 1989. On linear versus nonlinear flow rules in strain localization analysis. *Meccanica*, vol. 24, pp. 36–41.

Carol, I., Rizzi, E., & Willam, K., 1994. A unified theory of elastic degradation and damage based on a loading surface. *International Journal of Solids and Structures*, vol. 31, n. 20, pp. 2835–2865.

Cosserat, E. & Cosserat, F., 1909. *Théorie des corps déformables*. Hermann et fils, Paris. (in french).

de Borst, R., 1991. Simulation of strain localization: a reappraisal of the Cosserat continuum. *Engineering Computations*, vol. 8, n. 4, pp. 317–332.

de Borst, R. & Mühlhaus, H. B., 1992. Gradient-dependent plasticity: formulation and algorithmic aspects. *International Journal for Numerical Methods in Engineering*, vol. 35, pp. 521–539.

de Borst, R. & Sluys, L. J., 1991. Localization in a cosserat continuum under static and dynamic loading. *Computer Methods in Applied Mechanics and Engineering*, vol. 90, n. 1-3, pp. 805–827.

de Borst, R., Sluys, L. J., Muhlhaus, H. B., & Pamin, J., 1993. Fundamental issues in finite element analysis of localization of deformation. *Engineering Computations*, vol. 10, n. 2, pp. 99–121.

Desoyer, T. & Cormery, F., 1994. On uniqueness and localization in elastic-damage materials. *International Journal of Solids and Structures*, vol. 31, n. 5, pp. 733–744.

Dietsche, A., Steinmann, P., & Willam, K., 1993. Micropolar elastoplasticity and its role in localization. *International Journal of Plasticity*, vol. 9, pp. 813–831.

Ding, J. & Zhou, A., 2007. Eigenvalues of rank-one updated matrices with some applications. *Applied Mathematics Letters*, vol. 20, n. 12, pp. 1223 – 1226.

Dugdale, D. S., 1960. Yielding of steel sheets containing slits. *Journal of the Mechanics and Physics of Solids*, vol. 8, pp. 100–108.

Eremeyev, V. A., 2005. Acceleration waves in micropolar elastic media. *Doklady Physics*, vol. 50, n. 4, pp. 204–206.

Gori, L., Penna, S. S., & Pitangueira, R. L. S., 2017a. Discontinuous failure in micropolar elastic-degrading models. *International Journal of Damage Mechanics*, vol. 0, n. 0. (in press).

Gori, L., Penna, S. S., & Pitangueira, R. L. S., 2017b. An enhanced tensorial formulation for elastic degradation in micropolar continua. *Applied Mathematical Modelling*, vol. 41, pp. 299–315.

Gori, L., Pitangueira, R. L. S., Penna, S. S., & Fuina, J. S., 2015. A theoretical and computational framework for isotropic damage models based on a generalized micro-polar continuum theory. In *Proceedings of the XXXVI Ibero-Latin American Congress on Computational Methods in Engineering*, Rio de Janeiro, Brazil. ABMEC - Brazilian Association of Computational Methods in Engineering.

Grioli, A. C., 1980. Propagazione di onde di accelerazione in un solido viscoelastico di Cosserat. *Rendiconti del Seminario Matematico della Università di Padova*, vol. 64, pp. 25–37. (in italian).

Hadamard, J., 1903. *Leçons sur la propagation des ondes et les équations de l'hydrodynamique*. A. Hermann, France. (in french).

Hill, R., 1962. Acceleration waves in solids. *Journal of the Mechanics and Physics of Solids*, vol. 10, pp. 1–16.

Hunter, J. D., 2007. Matplotlib: A 2d graphics environment. *Computing In Science & Engineering*, vol. 9, n. 3, pp. 90–95.

Iordache, M. M. & Willam, K., 1998. Localized failure analysis in elastoplastic cosserat continua. *Computer Methods in Applied Mechanics and Engineering*, vol. 121, n. 3-4, pp. 559–586.

Jirásek, M., 2007. Mathematical analysis of strain localization. *European Journal Of Environmental And Civil Engineering*, vol. 11, n. 7-8, pp. 977–991.

Maier, G. & Hueckel, T., 1979. Nonassociated and coupled flow rules of elastoplasticity for rock-like materials. *International Journal of Rock Mechanics and Mining Sciences & Geomechanics Abstracts*, vol. 16, n. 2, pp. 77 – 92.

Marigo, J., 1985. Modelling of brittle and fatigue damage for elastic material by growth of microvoids. *Engineering Fracture Mechanics*, vol. 21, n. 4, pp. 861 – 874.

Needleman, A., 1988. Material rate dependence and mesh sensitivity in localization problems. *Computer Methods in Applied Mechanics and Engineering*, vol. 67, pp. 69–85.

Neilsen, M. & Schreyer, H., 1993. Bifurcations in elastic-plastic materials. *International Journal of Solids and Structures*, vol. 30, n. 4, pp. 521–544.

Ortiz, M., 1987. An analytical study of the localized failure modes of concrete. *Mechanics of Materials*, vol. 6, pp. 159–174.

Ottosen, N. S. & Runesson, K., 1991a. Acceleration waves in elasto-plasticity. *International Journal of Solids and Structures*, vol. 28, n. 2, pp. 135–159.

Ottosen, N. S. & Runesson, K., 1991b. Properties of discontinuous bifurcation solutions in elasto-plasticity. *International Journal of Solids and Structures*, vol. 27, n. 4, pp. 401–421.

Peerlings, R. H. J., 1999. *Enhanced damage modelling for fracture and fatigue*. PhD thesis, Technische Universiteit Eindhoven, Eindhoven, The Netherlands.

Peerlings, R. H. J., de Borst, R., Brekelmans, W. A. M., & de Vree, H. P., 1996. Gradient enhanced damage for quasi-brittle materials. *International Journal for Numerical Methods in Engineering*, vol. 39, pp. 3391–3403.

Peerlings, R. H. J., de Borst, R., Brekelmans, W. A. M., & Geers, M. G. D., 2002. Localization issues in local and nonlocal continuum approaches to fracture. *European Journal of Mechanics A/Solids*, vol. 115, n. 2, pp. 175–189.

Peerlings, R. H. J., Geers, M. G. D., de Borst, R., & Brekelmans, W. A. M., 2001. A critical comparison of nonlocal and gradient-enhanced softening continua. *International Journal for Numerical Methods in Engineering*, vol. 38, pp. 7723–7746.

Pijaudier-Cabot & Bažant, Z. P., 1987. Non-local damage theory. *Journal of Engineering Mechanics*, vol. 113, pp. 1512–1533.

Rahaman, M., Deepu, S., Roy, D., & Reddy, J., 2015. A micropolar cohesive damage model for delamination of composites. *Composite Structures*, vol. 131, pp. 425 – 432.

Rice, J. R., 1976. The localization of plastic deformation. In *Theoretical and Applied Mechanics - Proceedings of the 14th International Congress on Theoretical and Applied Mechanics*, Delft, Holland.

Rice, J. R. & Rudnicki, J. W., 1980. A note on some features of the theory of localization of deformation. *International Journal of Solids and Structures*, vol. 16, pp. 597–605.

Rizzi, E., 1995. *Sulla localizzazione delle deformazioni in materiali e strutture*. PhD thesis, Dipartimento di Ingegneria Strutturale, Politecnico di Milano, Milano, Italy. (in italian).

Rizzi, E. & Carol, I., 2001. A formulation of anisotropic elastic damage using compact tensor formalism. *Journal of Elasticity*, vol. 64, n. 2, pp. 85–109.

Rizzi, E., Carol, I., & Willam, K., 1995. Localization analysis of elastic degradation with application to scalar damage. *Journal of Engineering Mechanics*, vol. 121, n. 4, pp. 541–554.

Rizzi, E., Maier, G., & Willam, K., 1996. On failure indicators in multi-dissipative materials. *International Journal of Solids and Structures*, vol. 33, n. 20-22, pp. 3187–3214.

Rudnicki, J. & Rice, J., 1975. Conditions for the localization of deformation in pressure-sensitive dilatant materials. *Journal of the Mechanics and Physics of Solids*, vol. 23, pp. 371–394.

Sluys, L. J., 1992. *Wave propagation, localization and dispersion in softening solids*. PhD thesis, Technische Universiteit Delft, Delft, The Nederlands.

Steinmann, P., 1995. Theory and numerics of ductile micropolar elastoplastic damage. *International Journal for Numerical Methods in Engineering*, vol. 38, pp. 583–606.

Szabó, L., 2000. Comments on loss of stong ellipticity in elastoplasticity. *International Journal of Solids and Structures*, vol. 37, pp. 3775–3806.

Thomas, T. Y., 1961. *Plastic flow and fracture of solids*. Accademic Press, London.

Xotta, G., Beizaee, S., & Willam, K. J., 2016. Bifurcation investigation of coupled damage-plasticity models for concrete materials. *Computer Methods in Applied Mechanics and Engineering*, vol. 298, pp. 428–452.

Yang, Y. B. & Shieh, M. S., 1990. Solution method for nonlinear problems with multiple critical points. *AIIA Journal*, vol. 28, n. 12, pp. 2110–2116.